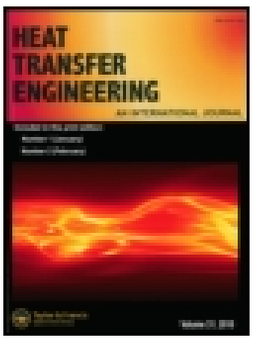

Heat Transfer Engineering

ISSN: 0145-7632 (Print) 1521-0537 (Online) Journal homepage: http://www.tandfonline.com/loi/uhte20

Natural Convection in a Trapezoidal Enclosure Heated from the Side with a Baffle Mounted on Its Upper Inclined Surface

F. MOUKALLED & M. DARWISH

To cite this article: F. MOUKALLED & M. DARWISH (2004) Natural Convection in a Trapezoidal Enclosure Heated from the Side with a Baffle Mounted on Its Upper Inclined Surface, Heat Transfer Engineering, 25:8, 80-93, DOI: 10.1080/01457630490520356

To link to this article: http://dx.doi.org/10.1080/01457630490520356

Heat Transfer Engineering, 25(8):80–93, 2004

ISSN: 0145-7632 print / 1521-0537 online
DOI: 10.1080/01457630490520356

Taylor & Francis
Taylor & Francis Group

Natural Convection in a Trapezoidal Enclosure Heated from the Side with a Baffle Mounted on Its Upper Inclined Surface

F. MOUKALLED and M. DARWISH

Department of Mechanical Engineering, American University of Beirut, Lebanon

A numerical investigation examined the effects on heat transfer of mounting baffles to the upper inclined surfaces of trapezoidal cavities. Two thermal boundary conditions are considered. In the first, the left, short vertical wall is heated while the right, long vertical wall is cooled (buoyancy assisting mode along the upper inclined surface of the cavity). In the second, the right, long vertical wall is heated while the left, short vertical wall is cooled (buoyancy opposing mode along the upper inclined surface of the cavity). For each boundary condition, computations are performed for three baffle heights, two baffle locations, four Rayleigh number values, and three Prandtl number values. Results are displayed in terms of streamlines, isotherms, and local and average Nusselt number values. For both boundary conditions, predictions reveal a decrease in heat transfer in the presence of baffles, with its rate generally increasing with increasing baffle height and Prandtl number. For a given baffle height, a higher decrease in heat transfer is generally obtained with baffles located close to the short vertical wall. Average Nusselt number correlations for both boundary conditions are presented.

Work on natural convection in enclosures is still the subject of numerous investigations due to its relevance to many heat transfer applications. Previous effort (as reviewed in [1]) has been biased towards analyzing this transfer phenomenon in regular shaped enclosures (e.g., rectangular, cylindrical, annulus). Few irregular shaped enclosures that are of practical importance (such as in solar heating, solidification, or nuclear waste disposal) have been studied. The irregular boundaries in such enclosures, coupled with the governing non-linear conservation equations, result in fundamental solutions specific to the configurations at hand and difficult to envisage a priori from solutions obtained in regular enclosures. This article reports on a numerical study conducted to explore the effects of baffle height and location on the total heat transfer in partially divided trapezoidal enclosures heated from the side with baffles mounted on their upper inclined surfaces. The configuration under consideration may arise in heat transfer applications of practical interest, such as insulation, solar collection enclosures, cooling of electronic equipment, and others.

Iyican et al. [2, 3] presented experimental and numerical results for natural convection in an inclined trapezoidal cavity formed of parallel and cylindrical

The financial support provided by the Lebanese National Council for Scientific Research (LNCSR) through grant no. 323-040-32254 is gratefully acknowledged.

Address correspondence to Dr. F. Moukalled, Department of Mechanical Engineering, American University of Beirut, P.O. Box 11-0236, Riad El Solh, Beirut, Lebanon. E-mail: memouk@aub.edu.lb

cold top and hot bottom walls and plane adiabatic sidewalls. Lam et al. [4] reported similar experimental and numerical results for a trapezoidal cavity composed of two vertical adiabatic sidewalls, a horizontal hot bottom wall, and an inclined cold top wall. Karyakin [5] reported on transient natural convection in a trapezoidal cavity with parallel top and bottom walls and inclined sidewalls. Lee [6, 7] and Peric [8] presented numerical results (up to a Rayleigh number of 10^5) for laminar natural convection in trapezoidal enclosures of horizontal, insulated bottom and top walls and inclined sidewalls that are maintained at different uniform temperatures. Computations in the same geometry were carried out by Sadat and Salagnac [9] using a control volume-based finite element technique for values of Rayleigh number ranging from 10^3 to 2×10^5. Using the control volume method, further results in the same geometry were reported by Kuyper and Hoogendoorn [10] for Rayleigh numbers between 10^4 and 10^8.

Studies related to buoyancy-induced heat transfer in partially divided trapezoidal cavities are limited to the ones reported in [11–14]. In the work presented in [11, 12], Moukalled and Acharya dealt with natural convection heat transfer in a partially divided trapezoidal cavity with the partial divider being attached to either the lower horizontal base [11] or the upper inclined surface [12] of the cavity. In [13], however, two offset partial vertical dividers attached to the upper inclined surface and the lower horizontal base of the cavity were employed. For all configurations, two boundary conditions representing summer-like conditions (upper surface heated) and winter-like conditions (upper surface cooled) were used. Results presented showed that the presence of baffles decreases heat transfer. The study reported in [14] differs from the previous ones in the geometry and boundary conditions. In [11–13], the cavity was symmetric in the x-direction (i.e., computations were performed in the left half of the domain, and the symmetry boundary condition was applied along the right vertical boundary), and the upper inclined surface was either heated or cooled. In [14], the cavity was half the one studied in [11–13], and the left vertical boundary was a wall boundary. In addition, the upper inclined surface was insulated. Similar to the work in [11], the baffle was attached to the lower horizontal base of the enclosure. The configuration in the present study is similar to that in [14], with the baffle (as in [12]) being mounted on the upper inclined surface of the cavity. As discussed in the extensive review on the subject presented by Ostrach [1], internal flows are more complex to predict than external flows, due to the interaction between the boundary layer and core and that the core flow is very sensitive to the geometry and boundary conditions. This is inherent to all confined convection configurations. As such, any slight change in the geometry and/or boundary conditions may dramatically change the flow pattern within the cavity and justify the need to analyze this new configuration.

PHYSICAL MODEL AND GOVERNING EQUATIONS

A sketch of the physical situation under consideration is depicted in Figure 1a. The width of the cavity (L) is four times the height (H) of the short vertical wall. The inclination of the top of the cavity is fixed at 15°. Three baffle heights ($H_b = H^*/3$, $2H^*/3$, and H^* where H^* is the height of the cavity at the location of baffle) and two baffle locations ($L_b = L/3$ and $2L/3$) are considered. In all computations, the baffle thickness (W_b) is taken as $W_b = L/20$ to simulate a thin baffle. Moreover, two boundary conditions are analyzed. In the first, the left short vertical wall of the cavity is maintained at the uniform hot temperature T_h, and the right long vertical wall is maintained at the uniform cold temperature T_c. Since the height of the cavity increases in the direction of the rising fluid, this boundary condition corresponds to the buoyancy-assisting mode along the upper inclined plane. In the second, the left wall is cold (T_c), while the temperature of the right wall is T_h. This boundary condition corresponds to the buoyancy-opposing mode along the upper inclined surface. For both conditions, the effects of mounting a baffle on the upper inclined surface of the cavity (Figure 1a), on the amount of heat transferred across the cavity are investigated.

The transport equations are non-dimensionalized using the following dimensionless variables:

$$X = \frac{x}{H}, \quad Y = \frac{y}{H} \tag{1}$$

$$U = \frac{u}{\nu/H}, \quad V = \frac{v}{\nu/H} \tag{2}$$

$$P = \frac{p + \rho g y}{\rho(\nu/H)^2}, \quad \theta = \frac{T - T_c}{T_h - T_c} \tag{3}$$

Using the Boussinesq approximation and assuming the flow to be laminar, steady, and two-dimensional with constant fluid properties (except for the induced variations in the body force term), the dimensionless governing transport equations of mass, momentum, and energy are, respectively, written as:

$$\frac{\partial U}{\partial X} + \frac{\partial V}{\partial Y} = 0 \tag{4}$$

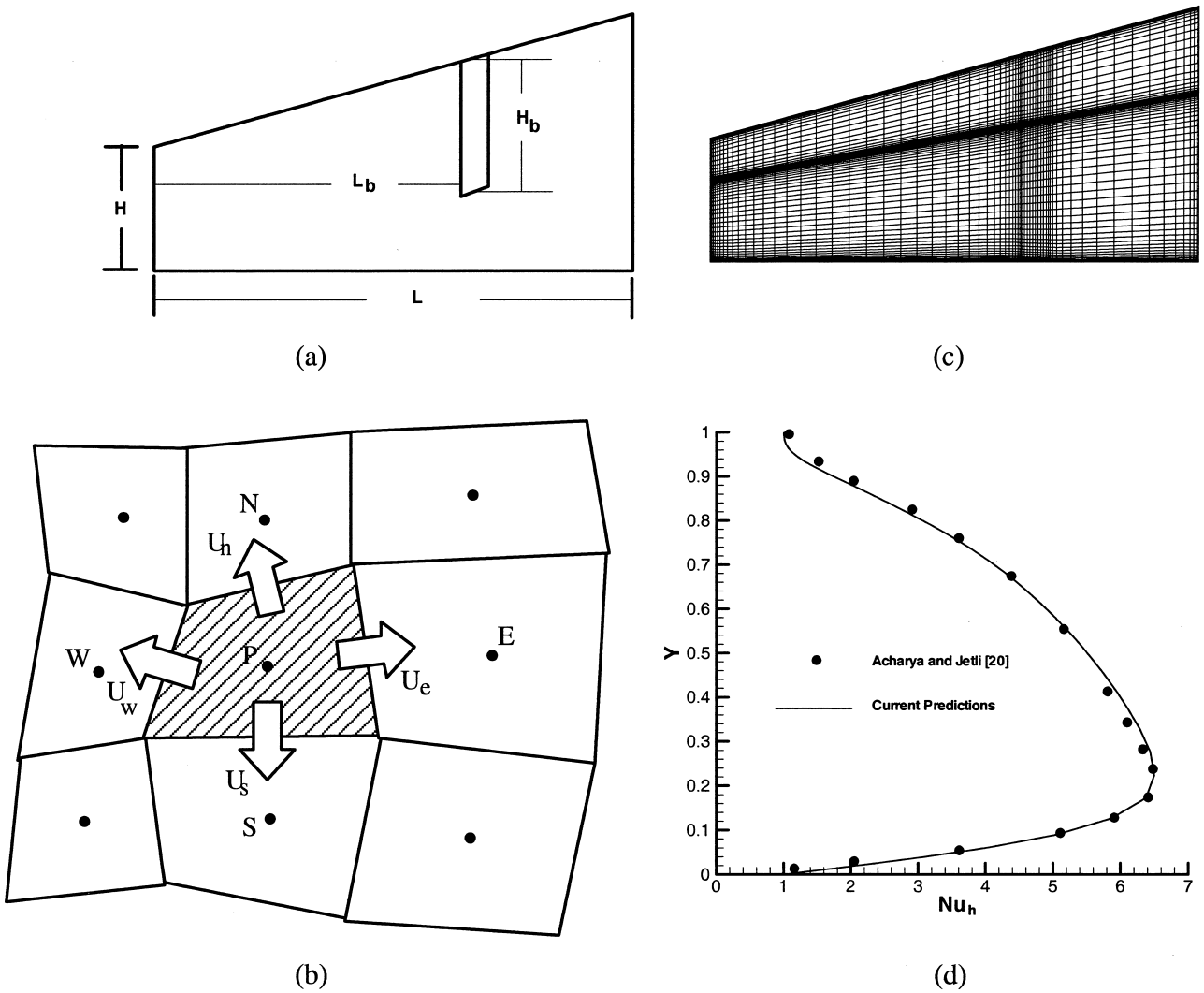

Figure 1 (a) Physical domain; (b) a typical control volume; (c) computational domain and an illustrative grid network; (d) comparison of predicted Nusselt number distribution along the hot wall of a partitioned square cavity against results published in [20].

$$U\frac{\partial U}{\partial X} + V\frac{\partial U}{\partial Y} = -\frac{\partial P}{\partial X} + \frac{\partial^2 U}{\partial X^2} + \frac{\partial^2 U}{\partial Y^2} \tag{5}$$

$$U\frac{\partial V}{\partial X} + V\frac{\partial V}{\partial Y} = -\frac{\partial P}{\partial Y} + \frac{\partial^2 V}{\partial X^2} + \frac{\partial^2 V}{\partial Y^2} + \frac{Ra \cdot \theta}{Pr} \tag{6}$$

$$U\frac{\partial \theta}{\partial X} + V\frac{\partial \theta}{\partial Y} = \frac{1}{Pr}\left[\frac{\partial^2 \theta}{\partial X^2} + \frac{\partial^2 \theta}{\partial Y^2}\right] \tag{7}$$

In the baffle region, the only conservation equation needed is the Laplace equation:

$$\frac{k_b/k}{Pr}\left[\frac{\partial^2 \theta_b}{\partial X^2} + \frac{\partial^2 \theta_b}{\partial Y^2}\right] = 0 \tag{8}$$

where k_b and θ_b denote the thermal conductivity and non-dimensional temperature in the baffle, respectively. The energy balance at the baffle–air interface can be stated as

$$-\frac{1}{Pr}\left(\frac{\partial \theta}{\partial n}\right)_i = -\frac{k_b/k}{Pr}\left(\frac{\partial \theta_b}{\partial n}\right)_i \tag{9}$$

where n is the direction normal to the baffle–air interface and the subscript i refers to the interface.

The associated flow and thermal boundary conditions are the no-slip condition on the enclosure walls, non-dimensional uniform temperatures of 1 and 0 along the hot and cold walls, and zero temperature gradient along the insulated walls.

SOLUTION PROCEDURE

The coupled system of equations governing the flow and temperature fields (Eqs. [4–7]) is solved

numerically using the control volume method. A collocated variables approach is adopted, and the special Momentum Weighted Interpolation Method for the calculation of the mass fluxes across the control volume faces [15] that embodies the SIMPLE algorithm of Patankar [16] is employed to suppress oscillatory checkerboard fields. In this procedure, the solution domain is subdivided into a number of control volumes, each associated with a grid point (Figure 1b). First integrating the equations over each control volume and then using Green's theorem to replace the volume integral by the surface integral will obtain the discretized forms. With suitable profile interpolation in each coordinate direction (the third order SMART scheme [17] is used and applied within the context of the NVSF methodology [18]) for the variables whose values are unknown on the control volume faces, a system of algebraic equations results that can be solved iteratively using a line-by-line Thomas algorithm. Pressure–velocity coupling is resolved through a guess-and-correct procedure similar to that described by Patankar [16]. Moreover, the grid is generated using the transfinite interpolation technique [19]. Furthermore, the presence of the baffle in the calculation domain is accounted for by the special treatment suggested by Patankar [16]. With this approach, the baffle region is treated as an infinitely viscous fluid (numerically specified as a very large value) with a nondimensional thermal conductivity corresponding to that of the baffle. This procedure leads to zero velocities in the baffle region, and the energy equation reduces to that of the Laplace heat conduction equation. Finally, since the control volume method guarantees overall conservation and conservation over each control volume in the domain (e.g., a flux leaving an east control volume face is exactly equal to the flux entering the west control volume face of the adjacent cell), arranging the control volume face to coincide with the divider interface ensures energy balance at the baffle–air interface and forces Eq. (9) to be implicitly satisfied.

Numerical Accuracy

To investigate the sensitivity of the solution to the grid used, numerical experiments were carried out with different sizes of non-uniform grids. A final 68×62 non-uniform mesh was used in generating all solutions presented in this work. The grid points were clustered close to solid boundaries where large gradients are expected (Figure 1c). The accuracy of the calculations was verified by comparing representative computed profiles of velocity, temperature, and local Nusselt number using the 68×62 non-uniform grid with those obtained on a 130×130 nearly uniform grid. The maximum difference between the two solutions in the various quantities predicted was smaller than 0.107%. Conservation for the various physical quantities was satisfied to within 0.00001% in each control volume. As a further check for the correctness of the solution procedure, computations were performed for $Ra = 3.55 \times 10^5$ in a partially divided square box of side L, for the case when a baffle of height L/2 positioned in the middle of the cavity is attached to the lower horizontal base of the cavity and results judged against data published in [20]. The comparison of the Nusselt number distribution along the vertical hot wall presented in Figure 1d indicates excellent agreement, given the error incurred while extracting values. In addition, the differences in the maximum value of the stream function and average Nusselt number in the cavity were found to be 0.78% and 0.45%, respectively.

RESULTS AND DISCUSSION

The parameters affecting heat transfer in this study are the Prandtl number (Pr), the Rayleigh number (Ra), the conductivity ratio (k_r), the baffle height (H_b), and the baffle location (L_b). For both boundary conditions, the following values are used: three Prandtl numbers (Pr = 0.7, 10, and 130), three baffle heights ($H_b = H^*/3$, $2H^*/3$, and H^*), two baffle locations ($L_b = L/3$ and $2L/3$), and Rayleigh number values varying between 10^3 and 10^6. Moreover, the conductivity ratio is fixed at 2 to simulate a poorly conducting divider.

In order to reveal the effects of the various parameters on heat transfer, results are presented in terms of streamline and isotherm plots and local and average Nusselt number values.

Buoyancy-Assisting Flow Along the Top Inclined Surface of the Enclosure

Streamlines and Isotherms

Figure 2 shows streamline and isotherm maps in a baffle-free enclosure for Pr = 0.7. As depicted, the flow structure consists of a single eddy rotating clockwise. At low Ra values, the eye of the recirculating vortex is close to the vertical cold wall of the enclosure, where the largest velocities are located (Figures 2a and 2b). As Ra increases (Figures 2c and 2d), the eye moves away from the cold wall toward the middle of the domain and upward toward the top inclined plane of the cavity. In addition, at the highest Ra value ($Ra = 10^6$), the flow separates near the lower right corner of the cavity, which is opposite to the behavior reported in [11, 12]. At a low Ra ($Ra = 10^3$, Figure 2e), isotherm values

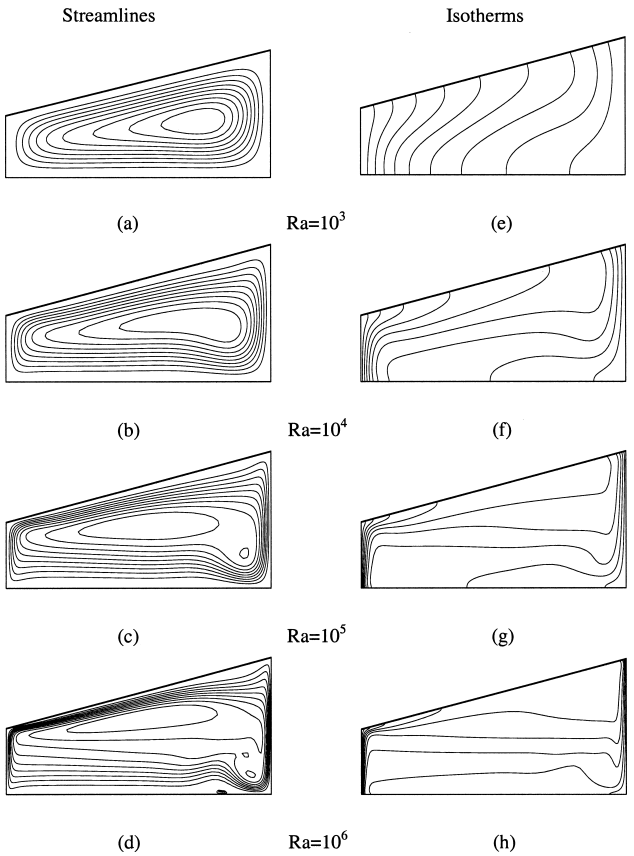

Figure 2 Streamline and isotherm plots in a non-partitioned cavity for the buoyancy assisting boundary condition.

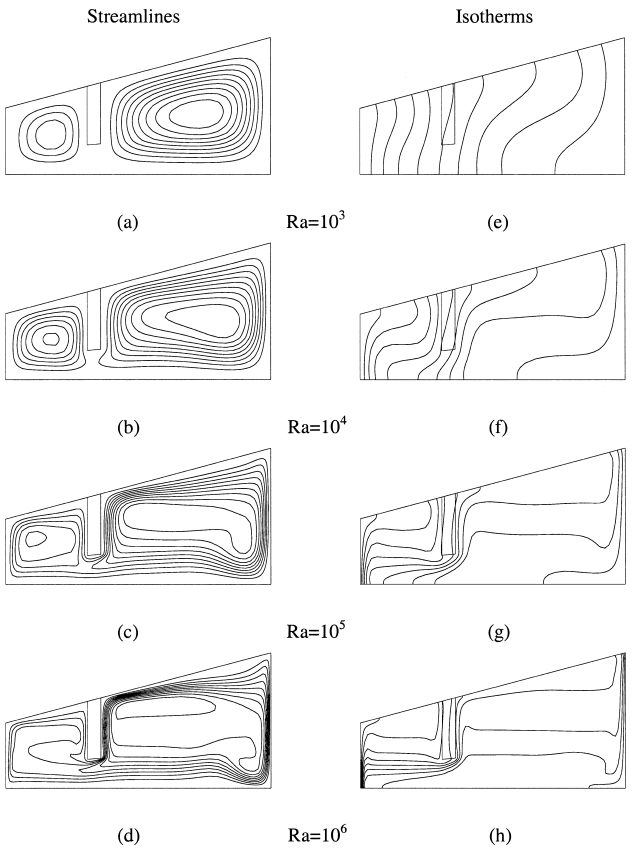

Figure 3 Streamline and isotherm plots ($H_b = 2H^*/3, L_b = L/3$) for the buoyancy assisting boundary condition.

decrease uniformly from hot to cold, showing dominant conduction heat transfer. As Ra values increase, the distribution of isotherms implies higher stratification levels within the enclosure (compare Figures 2e–2h) and consequently higher convection contribution. In addition, the boundary layer-type flow along the hot and cold wall becomes clearer.

The effects of partitioning the trapezoidal cavity on the flow patterns and temperature distributions are depicted in Figure 3 for $L_b = L/3$, $H_b = 2H^*/3$ and in Figure 4 for $L_b = 2L/3$, $H_b = 2H^*/3$. Streamlines in Figure 3 indicate that at low Ra ($Ra = 10^3$), the recirculating flow exhibits two clockwise rotating vortices with little communication between them (Figure 3a). As Ra increases, the interaction between the vortices increases until $Ra = 10^6$, when the two vortices merge into one (Figure 2d). Moreover, with increasing Ra values, the eye of the vortex in the right-hand portion of the domain moves upward and to the left as a result of increasing stratification levels in the lower right portion of the enclosure. Due to the weakness of the recirculating flow at reentry to the left portion of the domain and contrary to findings in [14], no jet-like flow is observed.

Isotherms presented in Figures 3e–3h reflect these flow patterns. At low Ra, variations in temperature are almost uniform over the domain, indicating a dominant conduction heat transfer mode. As Ra increases, convection is promoted, and stratification effects are increased.

The effects of positioning the baffle closer to the cold vertical wall on the velocity and temperature fields are depicted in Figure 4 ($L_b = 2L/3$, $H_b = 2H^*/3$). At low Ra values (Figures 4a and 4b), the flow structure is qualitatively similar to that presented in Figures 3a and 3b. As Ra values increase (Figures 4c and 4d), stratification levels increase, and isotherms become more distorted in the baffle-cold wall region as compared to the configuration in which the baffle is closer to the hot wall (Figures 3c and 3d). This indicates stronger convection caused by higher buoyancy effects as a result of the longer distance the flow travels before encountering the baffle. The above described behavior is further exemplified by the isotherm plots presented in Figures 4e–4h. At $Ra = 10^3$ (Figure 4e), stratification effects are small, and the distribution of isotherms is more or less uniform. As Ra increases, isotherms become more distorted (Figures 4f–4h), and stratification effects are promoted (Figures 4g and 4h).

Figure 5 shows the effects of baffle height ($H_b = 0$, $H^*/3$, $2H^*/3$, and H^*) on the hydrodynamic and thermal

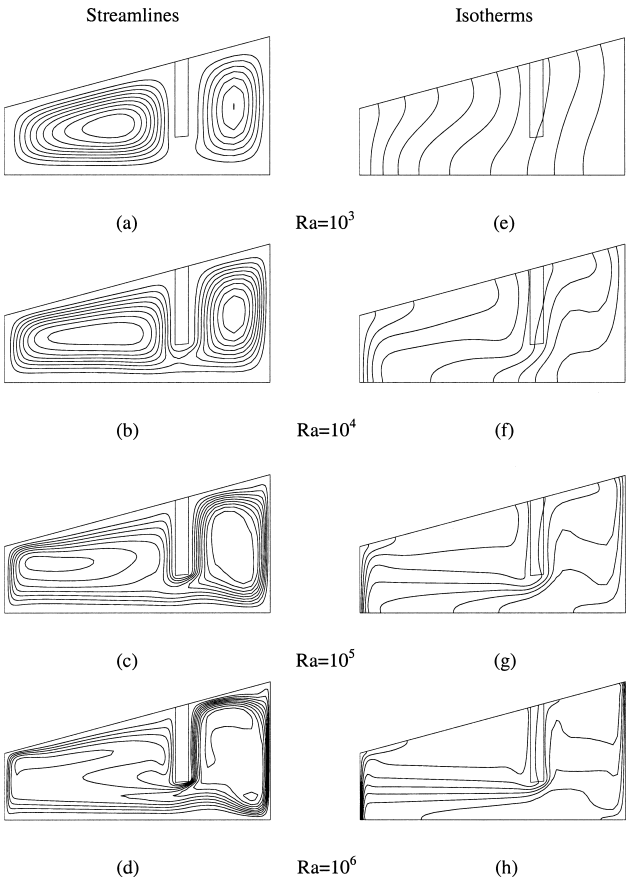

Figure 4 Streamline and isotherm plots ($H_b = 2H^*/3$, $L_b = 2L/3$) for the buoyancy assisting boundary condition.

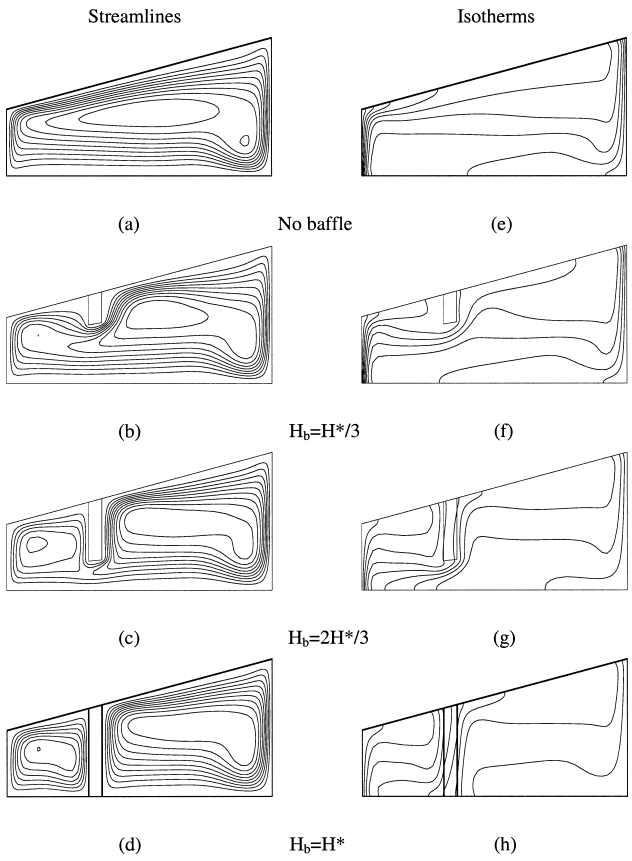

Figure 5 Streamline and isotherm plots ($Ra = 10^5$, $L_b = L/3$) at different H_b for the buoyancy assisting boundary condition.

fields in an enclosure with a divider located at $L_b = L/3$ and for $Ra = 10^5$. As H_b increases, a weaker flow is observed in both the right and left portions of the domain. For a fully partitioned enclosure (Figure 5d), two similar clockwise rotating eddies are noticed with their strength lower than the single vortex flow in the non-partitioned cavity due to a smaller convective area in each part combined with a decrease in the available temperature difference. Isotherms presented in Figures 5e–5h are in accordance with above findings and clearly show the decrease in convection heat transfer through the spread of isotherms.

The maximum absolute values of the stream function $|\psi_{max}|$ displayed in Table 1 indicate that the flow strength (maximum velocity in the domain) generally decreases with increasing baffle height and increasing values of Pr due to the increase in the fluid viscosity ($Pr = \mu c_p/k$). Moreover, the strength of the flow increases with Ra due to an increase in the temperature difference and consequently in buoyancy forces. At low and moderate Rayleigh number values, the maximum flow strength in a baffle-free enclosure is higher than its counterpart in a partitioned cavity. At high Ra, however, this may not be the case due to the formation of stronger vortices that operate over smaller convective areas.

Nusselt Numbers

The local and average Nusselt numbers along the hot or cold wall are computed using the following definitions:

$$Nu = h\ell/k \quad \overline{Nu} = \frac{1}{\ell}\int_0^{\ell} Nu\,dx \tag{10}$$

where ℓ is the height of the hot or cold wall. Based on this definition, the average Nusselt numbers along both walls are equal. Moreover, the heat transfer coefficient h is defined as

$$\dot{Q} = hA\,(T_h - T_c) = -kA\frac{dT}{dx} \Rightarrow h = -\frac{k}{H}\frac{d\theta}{dX} \tag{11}$$

Local Nusselt number variations (Nu) along the hot and cold sidewalls are presented in Figure 6. Values are plotted as a function of Y/Y_{max} where $Y_{max} = \ell$ is the height of the hot or cold vertical wall.

The Nu distributions along the hot and cold walls in a baffle free enclosure are compared in Figures 6a and 6b, respectively, against profiles obtained in a partitioned enclosure of baffle height $H_b = 2H^*/3$ located at $L_b = L/3$. As shown, the Nu levels increase with

Table 1 Maximum absolute values of the stream function for hot left (short) wall and cold right (tall) wall (buoyancy assisting boundary condition)

		$L_b = L/3$			$L_b = 2L/3$		
Ra	No baffle	$H_b = H^*/3$	$H_b = 2H^*/3$	$H_b = H^*$	$H_b = H^*/3$	$H_b = 2H^*/3$	$H_b = H^*$
				Pr = 0.7			
10^3	4.1	3.721	3.575	3.56	2.677	2.51	2.53
10^4	13.78	12.832	10.517	10.42	13.183	9.491	9.02
10^5	29.83	29.982	23.394	19.18	28.532	22.998	18.33
10^6	55.58	54.523	50.549	34.33	52.409	49.503	32.96
				Pr = 10			
10^3	0.29	0.2604	0.2506	0.25	0.1872	0.176	0.18
10^4	1.05	0.9721	0.7744	0.77	0.9684	0.6685	0.63
10^5	2.48	2.466	1.945	1.62	2.487	1.97	1.42
10^6	4.67	4.813	4.314	2.83	4.804	4.337	2.53
				Pr = 130			
10^3	0.022	0.020	0.01928	0.019	0.0144	0.01354	0.014
10^4	0.081	0.0752	0.05981	0.059	0.07467	0.05138	0.049
10^5	0.196	0.191	0.1514	0.126	0.1962	0.1537	0.109
10^6	0.371	0.3761	0.3292	0.222	0.3918	0.3431	0.197

increasing Ra, indicating a higher convection contribution. Both the hot and cold walls have a sharp peak, which is more pronounced at higher Ra values, occurring at the lower and upper sections of the walls, respectively, where the cold and warm flows impinge directly onto them. The peak on the cold wall is sharper than the one on the hot wall due to the aiding effects of buoyancy along the upper inclined plane of the enclosure, which further increases the velocity of the hot fluid before impinging on the cold wall. At all Ra values, the profiles in a partitioned enclosure are below their counterparts in a baffle-free enclosure, implying, as expected, a decrease in convection heat transfer. The effects of baffle height on Nu distributions along the hot and cold walls are depicted in Figures 6c and 6d, respectively, in an enclosure with a baffle located at $L_b = L/3$ and for a Ra value of 10^5. As shown, the trends of variations in Nu along both walls are similar for all baffle heights, with the level of Nu decreasing with increasing H_b. The Nu estimates in an enclosure with a baffle of height $H_b = H^*/3$ are slightly lower than values in a baffle-free enclosure. However, a notable decrease is achieved as the baffle height is increased. This is revealed further by the average Nusselt number values displayed in Table 2, which show at high Ra values a significant reduction in heat transfer as the baffle height is increased. At the lowest

Table 2 Average Nusselt number values ($\overline{Nu}$) for hot left (short) wall and cold right (tall) wall (Buoyancy assisting boundary condition)

		$L_b = L/3$			$L_b = 2L/3$		
Ra	No baffle	$H_b = H^*/3$	$H_b = 2H^*/3$	$H_b = H^*$	$H_b = H^*/3$	$H_b = 2H^*/3$	$H_b = H^*$
				Pr = 0.7			
10^3	0.715	0.5549	0.505	0.507	0.568	0.4934	0.492
10^4	2.48	2.021	1.133	1.108	2.249	1.316	1.224
10^5	5.476	5.122	3.023	2.136	5.359	3.672	2.404
10^6	10.925	10.488	7.457	3.648	10.754	8.659	4.162
				Pr = 10			
10^3	0.719	0.5567	0.506	0.508	0.568	0.494	0.493
10^4	2.666	2.138	1.17	1.142	2.355	1.355	1.258
10^5	6.102	5.622	3.253	2.2355	5.898	4.013	2.529
10^6	12.077	11.456	8.244	3.791	11.895	9.555	4.342
				Pr = 130			
10^3	0.719	0.5567	0.506	0.508	0.568	0.494	0.493
10^4	2.67	2.139	1.171	1.143	2.355	1.355	1.259
10^5	6.125	5.63	3.257	2.237	5.914	4.018	2.532
10^6	12.142	11.473	8.257	3.7954	11.948	9.57	4.347

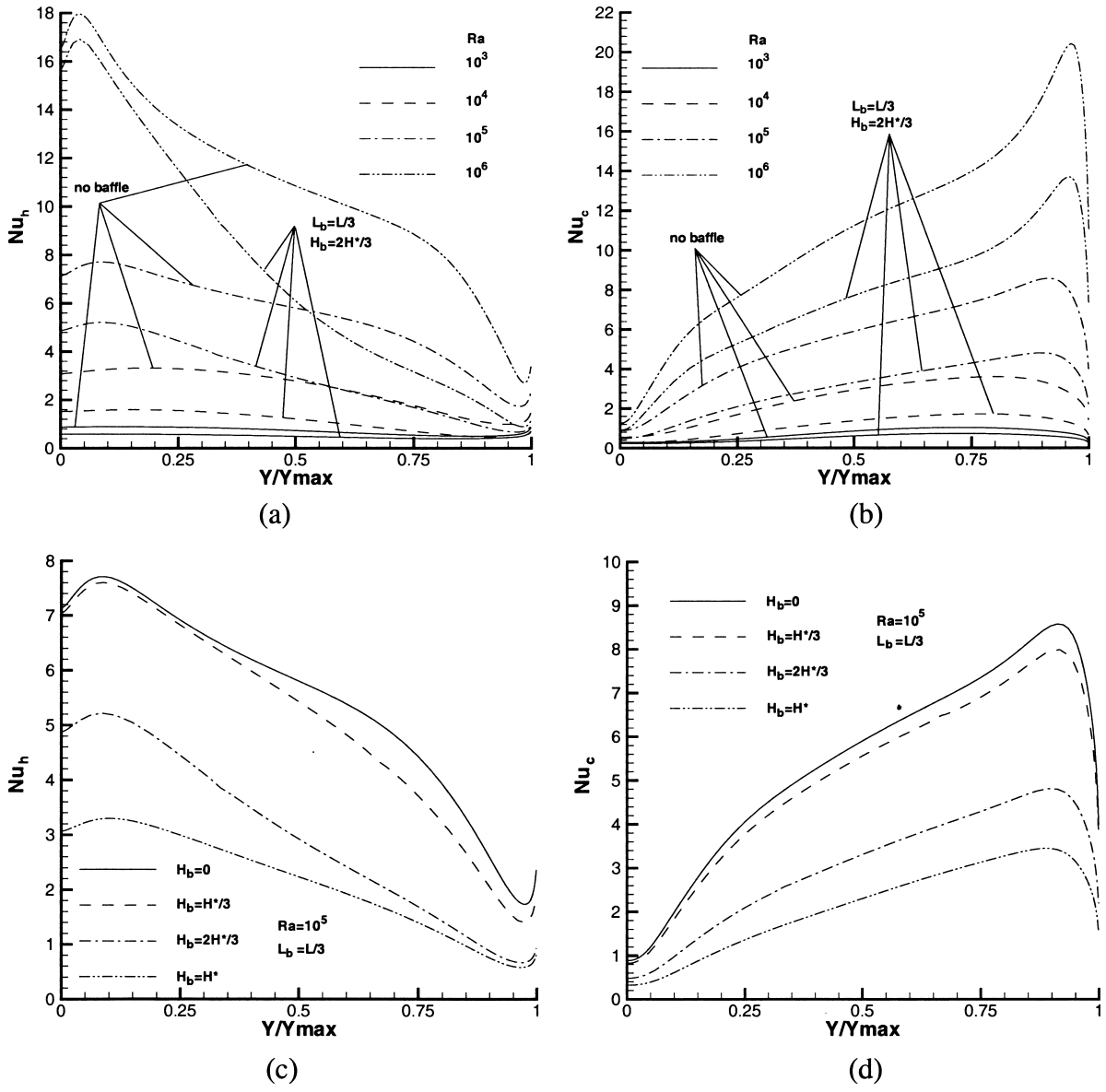

Figure 6 Local Nusselt number distribution along the hot (a, c) and cold (b, d) walls for the buoyancy assisting boundary condition.

Ra considered (10^3) and for all Pr values, the $\overline{\mathrm{Nu}}$ values are seen to minimize at a certain baffle height. Since convection contribution to total heat transfer is low at low Ra values, the increase in conduction within the enclosure as the baffle height is increased overwhelms the decrease in convection, and the net effect is an increase in total heat transfer. For a given baffle height, the total heat transfer increases with increasing Ra values due to an increase in convection heat transfer. Ratios of the partially divided enclosure Nusselt numbers to those of an open enclosure at the same Rayleigh number (Pr = 0.7) reveals that at the higher Rayleigh numbers, the percentage reduction in heat transfer varies from about 6.46% at $H_b = H^*/3$ to 66.61% at $H_b = H^*$ when the baffle is located at $L_b = L/3$, and from about 2.14% at $H_b = H^*/3$ to 61.9% at $H_b = H^*$ when $L_b = 2L/3$. Moreover, $\overline{\mathrm{Nu}}$ increases with increasing Pr due to a decrease in the thermal boundary layer thickness along the walls with a consequent increase in the temperature gradient, and the rate of increase rises with increasing Rayleigh number and falls with increasing Prandtl number.

The average Nusselt number values displayed in Table 2 are correlated with a maximum deviation of less than ±6.95% via the following relation (δ is the Dirac delta function):

$$\mathrm{Nu} = \delta\left(\frac{\mathrm{Ra}}{10^3} - 1\right)\mathrm{f}_1 + \delta\left(\frac{\mathrm{Ra}}{10^4} - 1\right)\mathrm{f}_2 + \delta\left(\frac{\mathrm{Ra}}{10^5} - 1\right)\mathrm{f}_3 + \delta\left(\frac{\mathrm{Ra}}{10^6} - 1\right)\mathrm{f}_4 \qquad (12)$$

where

$$f_1 = 1.4072 + 0.9194 \sin\left(-18\frac{H_b}{H^*} + 4\right)$$

$$f_2 = 1.8483 - 0.7786 \sin \times \left(-14.806\frac{H_b}{H^*} + 18.52\frac{L_b}{L} - 8\right) - 0.1043 \cos\left(5\frac{L_b}{L} + 5\right)$$

$$f_3 = 4.0786 + 1.7870 \sin\left(-15\frac{H_b}{H^*} - 20\frac{L_b}{L} + 14\right) - 0.1222 \cos\left(\frac{H_b}{H^*} + 9\frac{L_b}{L} + 11\,Pr + 25\right)$$

$$f_4 = 3.7874 - 7.9225 \sin \times \left(-17.08\frac{H_b}{H^*} - 19\left(\frac{L_b}{L}\right)^{14} + 17.1\right) + 1.109 \sin\left(-19.09\frac{H_b}{H^*} + 12Pr^{-19} - 12\right)$$

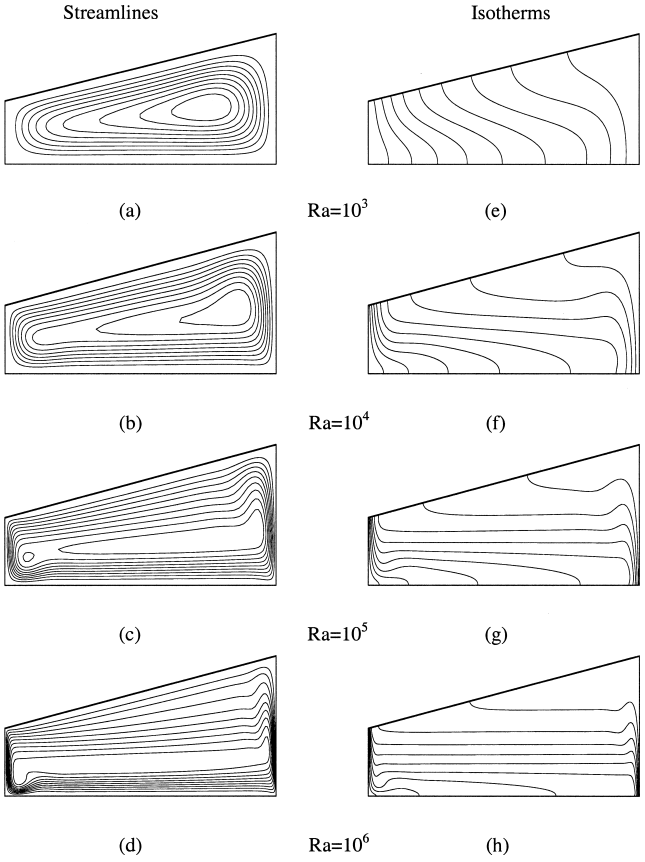

Figure 7 Streamline and isotherm plots in a non-partitioned cavity for the buoyancy opposing boundary condition.

Buoyancy-Opposing Flow Along the Top Inclined Surface of the Enclosure

Streamlines and Isotherms

Representative flow patterns and temperature distributions for Pr = 0.7 are depicted in Figures 7–10, and the maximum absolute values of the stream function $|\psi_{max}|$ are displayed in Table 3.

In the absence of baffles (Figure 7), the flow in the enclosure is composed of a single counterclockwise rotating cell. At low Ra, the eye of the recirculation is close to the vertical hot wall of the enclosure (Figures 7a and 7b). As Ra increases (Figures 7c and 7d), the eye elongates and separates into two vortices, one close to the hot wall and the other close to the cold wall.

At low Ra ($Ra = 10^3$), isotherms are uniformly distributed over the domain (Figure 7e), implying weak convection effects. As Ra increases, similar to the buoyancy assisting case, isotherms become more distorted and the mixing effects in the enclosure increase (compare Figures 7e–7h), indicating dominant convection heat transfer mode. In addition, the boundary layer-type flow along the hot and cold wall becomes clearer.

Streamline and isotherm maps for a partitioned enclosure are depicted in Figures 8–10. Unlike the buoyancy-aiding situation (Figures 3 and 4), streamlines indicate that the flow moves in a counterclockwise direction. Moreover, the flow neither separates nor stagnates on either side behind the divider. Furthermore, isotherms reveal high stratification levels (especially at high Ra values) on the top right-hand side of the domain where the hot rising fluid has to descend along the top inclined surface. By comparing results in Figure 8 against those reported in Figure 9, it can be inferred that placing the divider close to the hot wall has little effect on the global flow structure and thermal stratification in the enclosure. Figure 10 reveals the effects of baffle height in an enclosure with a divider located at $L_b = L/3$ and for $Ra = 10^5$. As the baffle height is increased, the flow becomes weaker, and a decrease in convection effects is observed, which is manifested by a lighter clustering of isotherms along the hot and cold walls.

The maximum absolute values of the stream function ψ_{max} displayed in Table 3 indicate that, like the buoyancy-aiding situation, the flow strength generally decreases with increasing baffle height, decreases with increasing values of Pr, and increases with Ra for the reasons stated earlier. Again, at low and moderate Rayleigh number values, the maximum flow strength in a baffle-free enclosure is higher than its counterpart in a partitioned cavity. At high Ra, however, this may not be the case, due to the formation of stronger vortices that operate over smaller convective areas.

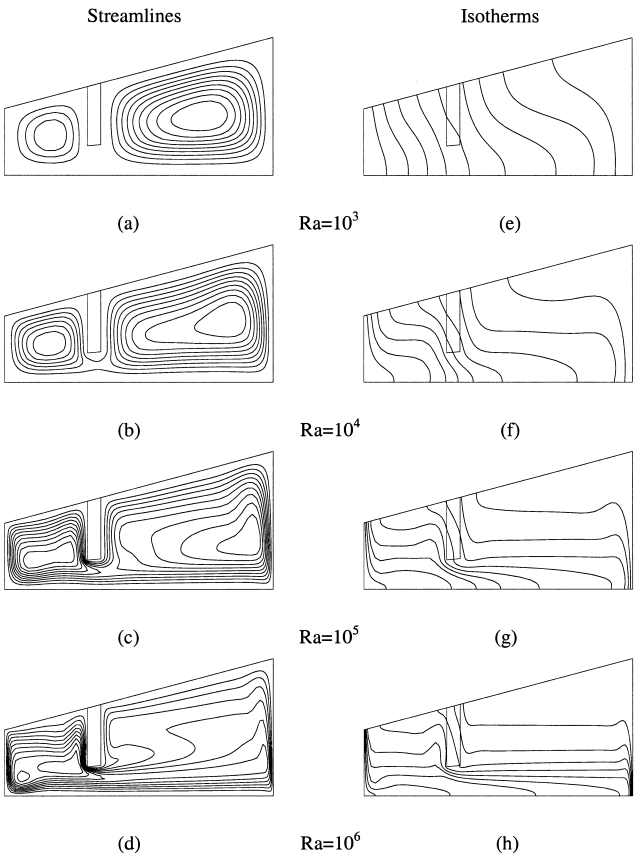

Figure 8 Streamline and isotherm plots ($H_b = 2H^*/3, L_b = L/3$) for the buoyancy opposing boundary condition.

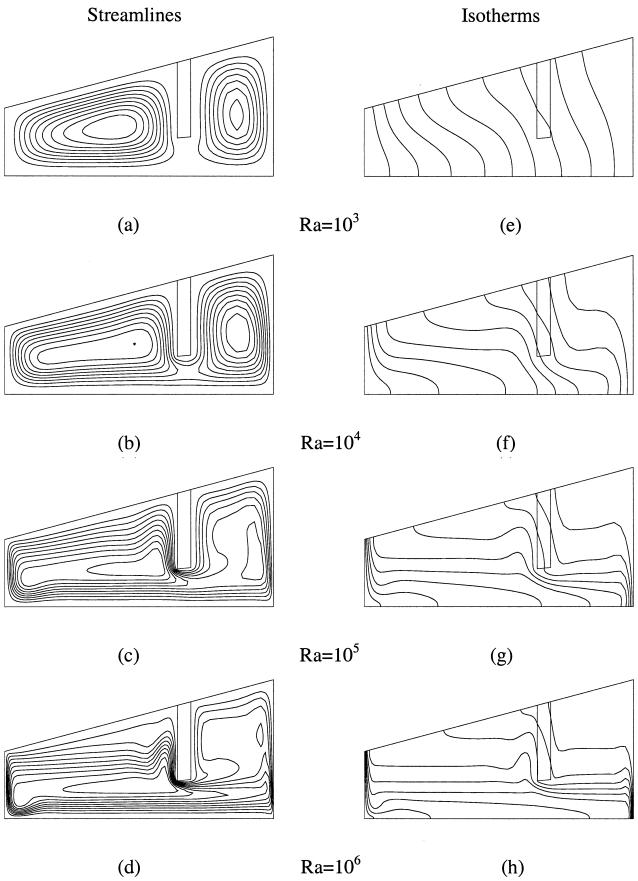

Figure 9 Streamline and isotherm plots ($H_b = 2H^*/3$, $L_b = 2L/3$) for the buoyancy opposing boundary condition.

Nusselt Numbers

The local and average Nusselt number values along the hot and cold walls are computed using Eqs. (10) and (11). The effects on heat transfer of partitioning the cavity can be assessed by a direct comparison between the Nu distributions along the hot and cold walls in a partitioned and a non-partitioned enclosure ($H_b = 2H^*/3$, $L_b = L/3$) that are displayed in Figures 11a–11d. The decrease in heat transfer in the presence of baffles can easily be depicted from the profiles presented

Table 3 Maximum absolute values of the stream function for cold left (short) wall and hot right (tall) wall (buoyancy opposing boundary condition)

		$L_b = L/3$			$L_b = 2L/3$		
Ra	No baffle	$H_b = H^*/3$	$H_b = 2H^*/3$	$H_b = H^*$	$H_b = H^*/3$	$H_b = 2H^*/3$	$H_b = H^*$
				Pr = 0.7			
10^3	3.32	3.1016	3.084	3.05	2.331	2.128	2.15
10^4	9.19	8.3847	7.7911	7.77	8.388	6.91	7.26
10^5	15.88	16.025	12.886	13.14	16.996	15.682	12.27
10^6	27.39	28.66	29.323	20.96	27.134	31.815	20.17
				Pr = 10			
10^3	0.23	0.218	0.217	0.21	0.169	0.149	0.15
10^4	0.68	0.613	0.569	0.57	0.606	0.475	0.51
10^5	1.33	1.244	1.005	1.04	1.341	1.273	0.91
10^6	2.34	2.372	2.532	1.67	2.34	2.753	1.44
				Pr = 130			
10^3	0.018	0.0168	0.0167	0.017	0.01262	0.0115	0.012
10^4	0.053	0.0472	0.0439	0.044	0.0467	0.0113	0.039
10^5	0.103	0.09643	0.0779	0.081	0.1039	0.099	0.07
10^6	0.183	0.18395	0.1977	0.129	0.1841	0.215	0.111

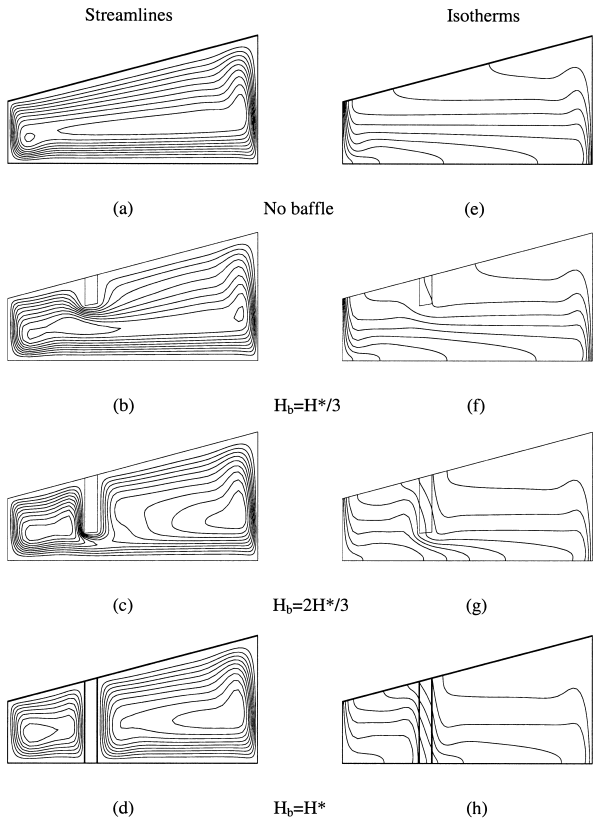

Figure 10 Streamline and isotherm plots ($Ra = 10^5$, $L_b = L/3$) at different H_b for the buoyancy opposing boundary condition.

in Figures 11a and 11b, where the Nu levels are seen to be higher in a baffle-free enclosure, especially at high Ra values where convection is the dominant heat transfer mode. As the fluid flows down the left cold wall, its temperature decreases, causing a decrease in heat transfer and consequently in Nu (Figure 11a). The high Nu value near $Y/Y_{max} = 1$ (Figure 11a) is due to the large temperature difference between the hot fluid and the cold wall. As the fluid moves up along the hot wall, its temperature increases and the temperature difference between the fluid and the hot wall decreases. This results in a decrease in Nu values, as depicted in Figure 11b. The peak at the leading edge of the hot wall is caused by the impingement of the cold fluid on the hot wall while trying to negotiate the corner. Moreover, Figures 11c and 11d ($Ra = 10^5$, $L_b = L/3$) reveal that the effect of increasing the baffle height is to decrease the Nu values along the hot and cold walls and, consequently, to reduce heat transfer.

The average Nusselt number values for all cases studied are displayed in Table 4. Predictions indicate a decrease in heat transfer in the presence of baffles. For $Ra = 10^3$ and for all Pr values, the increase in conduction overwhelms the decrease in convection as the baffle height is increased, resulting in an optimum baffle height for which $\overline{Nu}$ is minimum. For $Ra \geq 10^4$, however, the decrease in heat transfer increases with increasing baffle height for all Pr values considered. Moreover, for a given baffle height, the total heat transfer increases with increasing Ra due to an increase in convection heat transfer. At $Ra = 10^6$ and $Pr = 0.7$, the percent reduction in heat transfer varies from about 4.58% at $H_b = H^*/3$ to 63.74% at $H_b = H^*$ when the baffle is located at $L_b = L/3$, and from about 2.23% at $H_b = H^*/3$ to 60.44% at $H_b = H^*$ when $L_b = 2L/3$. As in the buoyancy-assisting case, $\overline{Nu}$ increases with increasing Pr due to a decrease in the thermal boundary layer thickness along the walls with a consequent increase in the temperature gradient.

The average Nusselt number values displayed in Table 4 are correlated with a maximum deviation of less

Table 4 Average Nusselt number values ($\overline{Nu}$) for cold left (short) wall and hot right (tall) wall (buoyancy opposing boundary condition)

		$L_b = L/3$			$L_b = 2L/3$		
Ra	No baffle	$H_b = H^*/3$	$H_b = 2H^*/3$	$H_b = H^*$	$H_b = H^*/3$	$H_b = 2H^*/3$	$H_b = H^*$
				Pr = 0.7			
10^3	0.6153	0.51	0.481	0.484	0.523	0.467	0.467
10^4	1.922	1.602	1.003	0.985	1.756	1.12	1.51
10^5	4.431	4.12	2.59	1.89	4.28	3.14	2.062
10^6	8.84	8.435	6.33	3.205	8.643	7.175	3.497
				Pr = 10			
10^3	0.617	0.511	0.48	0.4844	0.525	0.467	0.4668
10^4	1.986	1.642	1.017	0.998	1.805	1.141	1.0626
10^5	4.686	4.345	2.7	1.926	4.521	3.347	2.109
10^6	9.358	8.925	6.767	3.266	9.148	7.669	3.575
				Pr = 130			
10^3	0.617	0.511	0.4815	0.4845	0.525	0.467	0.4668
10^4	1.988	1.643	1.017	0.998	1.805	1.142	1.063
10^5	4.694	4.349	2.701	1.927	4.526	3.3504	2.11
10^6	9.375	8.933	6.766	3.268	9.163	7.672	3.578

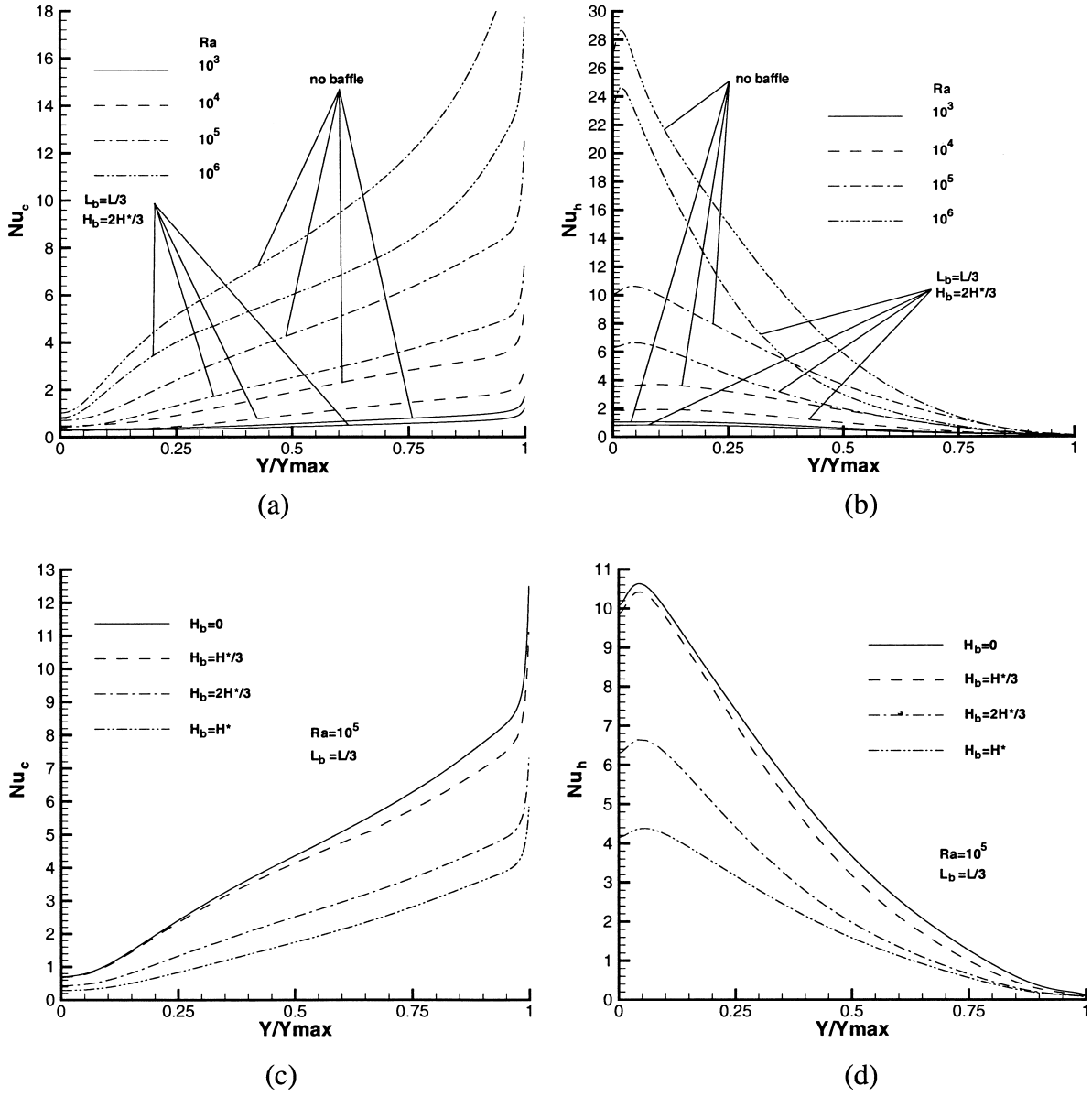

Figure 11 Local Nusselt number distribution along the hot (a, c) and cold (b, d) walls for the buoyancy opposing boundary condition.

than ±4.95% via the following relation (δ is the Dirac delta function):

$$\mathrm{Nu} = \delta\left(\frac{\mathrm{Ra}}{10^3} - 1\right)\mathrm{f}_1 + \delta\left(\frac{\mathrm{Ra}}{10^4} - 1\right)\mathrm{f}_2 + \delta\left(\frac{\mathrm{Ra}}{10^5} - 1\right)\mathrm{f}_3 + \delta\left(\frac{\mathrm{Ra}}{10^6} - 1\right)\mathrm{f}_4 \qquad (13)$$

where

$$\mathrm{f}_1 = 1.0681 + 0.6008\sin\left(-18\frac{\mathrm{H_b}}{\mathrm{H^*}} + 4\right)$$

$$\mathrm{f}_2 = 1.4899 + 0.5212\sin\left(-15\frac{\mathrm{H_b}}{\mathrm{H^*}} + 14\right) + 0.0825\cos\left(-2\frac{\mathrm{H_b}}{\mathrm{H^*}} - 12\frac{\mathrm{L_b}}{\mathrm{L}} - 23\right)$$

$$\mathrm{f}_3 = 3.2325 - 1.3614\sin\left(-23\frac{\mathrm{H_b}}{\mathrm{H^*}} + 20\frac{\mathrm{L_b}}{\mathrm{L}} - 20\right) + 0.1459\cos\left(-7\frac{\mathrm{H_b}}{\mathrm{H^*}} + 20\frac{\mathrm{L_b}}{\mathrm{L}} + 12\right)$$

$$\mathrm{f}_4 = 3.8795 - 5.2550\sin\left(-21\frac{\mathrm{H_b}}{\mathrm{H^*}} + 19\frac{\mathrm{L_b}}{\mathrm{L}} - 20\right) - 0.2674\cos\left(-2\frac{\mathrm{H_b}}{\mathrm{H^*}} - 17\frac{\mathrm{L_b}}{\mathrm{L}} - 20\,\mathrm{Pr} + 8\right)$$

CONCLUSIONS

Natural convection in a trapezoidal cavity heated from the side with a baffle mounted to its upper inclined surface has been studied numerically. In particular, the effects of the Rayleigh number, Prandtl number, baffle height, and baffle location on heat transfer were investigated for two boundary conditions representing buoyancy-assisting and buoyancy-opposing modes along the upper inclined surface of the cavity. For both boundary conditions, convection contribution to total heat transfer was found to increase with an increasing Rayleigh number. The presence of baffles decreased heat transfer, with its rate increasing by increasing both Pr and H_b. For the cases considered, a decrease in heat transfer as high as close to 70% was achieved.

NOMENCLATURE

A	surface area
c_P	specific heat of fluid
g	gravitational acceleration
h	heat transfer coefficient
H	height of the short vertical wall
H_b	baffle height
H^*	height of the cavity at the location of the baffle
k	thermal conductivity
k_b	baffle thermal conductivity
k_r	conductivity ratio, k_b/k
ℓ	height of the hot or cold wall
L	width of the cavity
L_b	baffle location
Nu	local Nusselt number
$\overline{Nu}$	average Nusselt number
p, P	dimensional and dimensionless pressure
Pr	Prandtl number ($= \mu c_P/k$)
$\dot{Q}$	rate of heat transfer
Ra	Rayleigh number ($= g\beta(T_h - T_c)H^3/\nu\alpha$)
T	dimensional temperature
u, U	dimensional and dimensionless horizontal velocity component
v, V	dimensional and dimensionless vertical velocity component
W_b	baffle thickness
x, X	dimensional and dimensionless coordinate along the horizontal direction
y, Y	dimensional and dimensionless coordinate along the vertical direction

Greek Symbols

α	thermal diffusivity, $k/\rho c_P$
β	coefficient of thermal expansion
δ	Dirac delta function
μ	viscosity
ν	kinematic viscosity, μ/ρ
θ	dimensionless temperature
θ_b	dimensionless baffle temperature
ρ	density
ψ	stream function

Subscripts

c	cold wall
h	hot wall
i	condition at baffle–air interface
max	maximum value

REFERENCES

[1] Ostrach, S., Natural Convection in Enclosures, *Journal of Heat Transfer*, vol. 110, pp. 1175–1190, 1988.

[2] Iyican, L., Bayazitoglu, Y., and Witte, L., An Analytical Study of Natural Convective Heat Transfer within a Trapezoidal Enclosure, *Journal of Heat Transfer*, vol. 102, pp. 640–647, 1980.

[3] Iyican, L., Witte, L. C., and Bayazitoglu, Y., An Experimental Study of Natural Convection in Trapezoidal Enclosures, *Journal of Heat Transfer*, vol. 102, pp. 648–653, 1980.

[4] Lam, S. W., Gani, R., and Simons, J. G., Experimental and Numerical Studies of Natural Convection in Trapezoidal Cavities, *Journal of Heat Transfer*, vol. 111, pp. 372–377, 1989.

[5] Karyakin, Y. E., Transient Natural Convection in Prismatic Enclosures of Arbitrary Cross-section, *Int. J. Heat Mass Transfer*, vol. 32, no. 6, pp. 1095–1103, 1989.

[6] Lee, T. S., Numerical Experiments with Fluid Convection in Tilted Nonrectangular Enclosures, *Numerical Heat Transfer, Part A*, vol. 19, pp. 487–499, 1991.

[7] Lee, T. S., Computational and Experimental Studies of Convective Fluid Motion and Heat Transfer in Inclined Nonrectangular Enclosures, *International Journal of Heat and Fluid Flow*, vol. 5, pp. 29–36, 1984.

[8] Peric, M., Natural Convection in Trapezoidal Cavities, *Numerical Heat Transfer, Part A*, vol. 24, pp. 213–219, 1993.

[9] Sadat, H., and Salagnac, P., Further Results for Laminar Natural Convection in a Two-dimensional Trapezoidal Enclosure, *Numerical Heat Transfer, Part A*, vol. 27, pp. 451–459, 1995.

[10] Kuyper, R. A., and Hoogendoorn, C. J., Laminar Natural Convection Flow in Trapezoidal Enclosures, *Numerical Heat Transfer, Part A*, vol. 28, pp. 55–67, 1995.

[11] Moukalled, F., and Acharya, S., Buoyancy-induced Heat Transfer in Partially Divided Trapezoidal Cavities, *Numerical Heat Transfer, Part A*, vol. 32, pp. 787–810, 1997.

[12] Moukalled, F., and Acharya, S., Natural Convection in Trapezoidal Cavities with Baffles Mounted on the Upper Inclined Surfaces, *Numerical Heat Transfer, Part A*, vol. 37, no. 6, pp. 545–565, 2000.

[13] Moukalled, F., and Acharya, S., Natural Convection in a Trapezoidal Enclosure with Offset Baffle, *AIAA Journal of Thermophysics and Heat Transfer*, vol. 15, no. 2, pp. 212–218, 2001.

[14] Moukalled, F., and Darwish, M., Natural Convection in a Partitioned Trapezoidal Cavity Heated from the Side, *Numerical Heat Transfer, Part A*, vol. 43, pp. 543–563, 2003.
[15] Peric, M., A Finite Volume Method for the Prediction of Three Dimensional Fluid Flow in Complex Ducts, Ph.D. thesis, Imperial College, Mechanical Engineering Department, London, 1985.
[16] Patankar, S. V., *Numerical Heat Transfer and Fluid Flow*, pp. 44–47, Hemisphere Publishing Corporation, New York, 1980.
[17] Gaskell, P. H., and Lau, A. K. C., Curvature Compensated Convective Transport: SMART, A New Boundedness Preserving Transport Algorithm, *Int. J. Num. Meth. Fluids*, vol. 8, pp. 617–641, 1988.
[18] Darwish, M., and Moukalled, F., Normalized Variable and Space Formulation Methodology For High-Resolution Schemes, *Numerical Heat Transfer, Part B*, vol. 26, pp. 79–96, 1994.
[19] Gordon, W. J., and Theil, L. C., Transfinite Mappings and Their Applications to Grid Generation, *Numerical Grid Generation*, ed. J. F. Thompson, pp. 171–192, North Holland, New York, 1982.
[20] Acharya, S., and Jetli, R., Heat Transfer Due to Buoyancy in a Partially Divided Square Box, *International Journal of Heat and Mass Transfer*, vol. 33, no. 5, pp. 931–942, 1990.

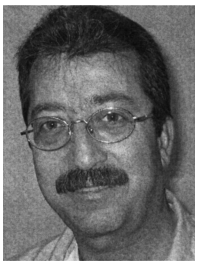

Fadl Moukalled is a professor of mechanical engineering at the American University of Beirut. He received his Ph.D. in 1987 from Louisiana State University, USA. His main research interests are computational fluid dynamics, numerical heat transfer, and finite time thermodynamics. Currently, his main research thrust is in all-speed multi-fluid and multi-phase systems.

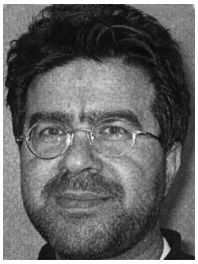

M. Darwish is a professor at the mechanical engineering department of the American University of Beirut. His research interest is in computational fluid dynamics, where he has worked on the development of high resolutions schemes, and in the development of pressure–velocity coupling algorithms for all-speed and multi-fluid flows.